HOKKAIDO UNIVERSITY

Title	Thickness distribution, texture and stratigraphy, and a simple probabilistic model for dynamical thickening of sea ice in the southern Sea of Okhotsk
Author(s)	Toyota, Takenobu; 豊田, 威信; Kawamura, Toshiyuki et al.
Description	An edited version of this paper was published by AGU. Copyright 2004, American Geophysical Union, "Journal Of Geophysical Research-oceans", Vol.109
Citation	Journal of Geophisical Research, 109, C06001 https://doi.org/10.1029/2003JC002090
Issue Date	2004-06-02
Doc URL	https://hdl.handle.net/2115/5565
Type	journal article
File Information	JGR109-C6.pdf

Title:

Thickness Distribution, Texture and Stratigraphy, and a simple probabilistic Model for

Dynamical Thickening of Sea Ice in the Southern Sea of Okhotsk

Takenobu Toyota[1], Toshiyuki Kawamura[1], Kay I.Ohshima[1], Haruhito Shimoda[2],

and Masaaki Wakatsuchi[1]

[1] Institute of Low Temperature Science, Hokkaido University

[2]National Maritime Research Institute, Japan

Running title: Growth processes of the Okhotsk sea ice

Abstract

Sea ice thickness data and sea ice samples were analyzed to examine the characteristics of the ice thickness distribution, ice texture, and to understand ice growth processes in the southern Sea of Okhotsk. Ice thickness data and samples were obtained aboard the icebreaker *SOYA* in early February, the ice growth season. Ice thickness data, which were obtained with a video monitoring system installed on the side deck of the ship each winter from 1991 to 2000 except 1995, show that the average thickness ranges from 19 ± 7 to 55 ± 23 cm and that it matches the characteristics of a Poisson distribution. Ice structure analysis reveals that granular texture occupies about three-quarters of the total ice thickness and that the ice exhibits a layered structure with unit thickness averaging 5 to 10cm. Stratigraphy and stable isotopic composition of the ice indicate that snow ice accounts for 10% and frazil ice 64% of the total ice thickness. This suggests that dynamic ice thickening processes such as frazil ice growth and piling-up are more significant than congelation growth. Based on these characteristics, which resemble more those of Antarctic than Arctic sea ice, we propose a conceptual model for the ice thickening process in this region. It is shown that this model can explain the shape of the ice thickness distribution well, and is analogous with the concept of the *pancake cycle* and multiple rafting of Antarctic sea ice growth and thickening.

1. Introduction

The ice thickness distribution is one of the controlling factors of heat exchange between atmosphere and ocean. As pointed out by *Maykut* [1978], the ice thickness distribution plays an important role in estimating turbulent flux in the Arctic ice area, particularly over thin ice, because the turbulent flux increases drastically with the decrease of ice thickness especially for ice <1m thick. *Worby and Allison* [1991] also showed that leads and thin ice have the impact on total heat exchange in the Antarctic. In the southern Sea of Okhotsk, *Toyota and Wakatsuchi* [2001] showed that thin ice and open water area contribute significantly to the total turbulent heat flux over the entire sea ice area. Therefore, ice thickness data are essential to the estimation of the heat budget over the ice cover in this region.

In addition, the ice thickness distribution has a dynamic influence on the large scale variation of sea ice because the deformation process depends largely on ice thickness. For example, it is easier for thin ice to be involved in ridging than for thick ice [*Thorndike et al.,* 1975]. This suggests that the ice thickness distribution has an impact on the strength of the ice pack and thereby can affect the variation of ice extent at large scales. Thus, the ice thickness distribution plays an important role in the interaction between atmosphere and ocean both dynamically and thermodynamically. However, quantitative ice thickness data have been very limited due to the lack of observations so far in the Sea of Okhotsk.

There had been no systematic observation in the Sea of Okhotsk before 1991, when the National Maritime Research Institute (NMRI) initiated ice thickness measurements to examine the effect of sea ice on ship navigation in ice-covered regions. The general statistics of the ice thickness distribution were reported by *Shimoda et al.* [1996] on the basis of the data from 1991 to 1994. Recently, ice profiling sonar measurements were conducted off the Hokkaido coast by *Fukamachi et al.* [2003]. Since the ice thickness distribution has a close relationship with ice growth processes, the former may provide a key to understand the latter.

In addition to ice thickness data, the structural analysis of ice samples is also indispensable to understand the growth processes of sea ice. For this purpose, the Institute of Low Temperature Science (ILTS) has been conducting systematic ice observations since 1996, including the measurement of ice thickness and ice concentration, ice sampling, and hydrographical and meteorological observations. To examine the structural characteristics of sea ice, about fifty samples of young ice and first-year ice were collected from 1996 to 2000. For each sample, thin section analysis was done to see the texture and stratigraphy, and the isotopic compositions (^{18}O) were measured to discriminate snow ice from ice grown from sea water. *Ukita et al.* [2000] reported first results of this work, mainly from 1996 data. The purpose of this paper is to present the results of ice thickness distribution and ice structure investigations between 1991 and 2000 and to present a dynamic model of the ice thickening process based on the observations made in the Sea of Okhotsk.

The theoretical relationship between ice thickening processes and the ice thickness distribution has been studied by numerous researchers. It is mainly dynamic processes, such as rafting and ridging, that generate ice thickness variations in a given area. (In this paper, we use the term 'dynamical process' in the meaning that the ice is formed under dynamical circumstances.) To formulate these dynamic processes, *Hibler et al.* [1972], for example, derived statistics of ridging properties theoretically using a stochastic model. *Thorndike et al.* [1975] introduced a redistribution function   to represent dynamic processes explicitly in sea ice models. *Thorndike* [1992] further tested their model with observations. *Thorndike* [2000] examined a simplified version of   to represent the observational fact that the thick end of the ice thickness distribution fits a negative exponential. However, both these theoretical approaches explained the ice thickness variations in the perennial ice regions. In the marginal ice zone (MIZ), where thin ice dominates, deformation processes seem to be different from those in the perennial ice regions, where sea ice of more than one meter thick is

prevalent [e.g. *Worby et al.*, 1996].

A substantial amount of field research on synoptic ice thickness distribution has been done so far in the polar regions. However, the observations have been done mainly for perennial or seasonal/thick ice regions. As for the MIZ, *Wadhams et al.* [1985], for example, showed the characteristics of the ice thickness distribution from submarine sonar data in the MIZ of Davis Strait. *Worby et al*. [1996] obtained ice thickness data from ship-based visual observations near the Antarctic. Even so, direct observations on ice thickness are still scarce. Thus, we may say that research on the ice thickness distribution in the MIZ is insufficient in terms of both observation and theory.

In the MIZ, located near the advancing sea-ice edge, the interaction between wind and ocean is vigorous, and probably affects ice thickening processes. For ice growth near the advancing sea-ice edge in the Antarctic, a *'pancake cycle'* has been proposed as a conceptual model by *Lange et al*. [1989]. Since the vast ice area of the seasonal ice zones (SIZ) is significantly occupied by the MIZ in early winter, the quantitative analysis of sea ice in the MIZ can lead to the understanding of the ice growth process in the SIZ. Therefore, we believe that the analysis of our data in our study area, located near the MIZ, also serves to explain the ice growth processes in the SIZ. In addition, because repeat measurements of ice thickness in the same area are very few even in the perennial ice zone, we consider that it is meaningful to show the results of our observations for nine years.

This paper is organized as follows. In the next section, we explain the measurement method. The results of ice thickness and ice   structure analysis will be shown in Section 3. In Section 4, a conceptual model for the ice thickening process is proposed on the basis of the observational results and then compared with other models. Finally, we summarize and discuss the results in Section 5.

2. Observation

Ice thickness measurement by means of video monitoring in the Sea of Okhotsk was initiated by NMRI in 1991. Since then measurements have been conducted every year except for 1995. From 1996 on, ILTS has carried out systematic ice observations aboard the icebreaker Patrol Vessel (P/V) *SOYA* in early February in the southern Sea of Okhotsk (Figure 1), in collaboration with the Japan Coast Guard. During these cruises, we made direct measurements of both meteorological and ice conditions, in particular ice concentration and thickness. In addition, we collected sea ice samples to investigate their crystallographic structure. The average meteorological conditions for 1996 to 2000 are listed in Table 1.

2.1 Ice thickness measurements

A video monitoring system was utilized for ice thickness measurements. We mounted a downward-looking video camera on the side deck of the ship to record the ice floes which broke at the bow and then turned into side-up positions alongside the hull (Figure 2). We searched for those ice floes that turned at right angles and the ice thickness was measured manually on each video image [*Toyota et al.*, 1999]. To determine the scale on the video images, crossed sticks of one meter length were lowered onto ice floes during the cruise. The reading error is considered to be less than a few centimeters at most. We consider that the sampling bias due to the ship's routes is also small because in most cases ice thickness was below one meter, which is within the ship's ice breaking ability, and the ship did not take the thinner ice routes. Therefore, the statistics of the ice thickness data are representative of the actual ice thickness distribution. However, it should be noted that ridged ice is beyond our measuring ability because its greater thickness and roughness prevents it from turning to the side-up position. This contrasts with measurements by upward-looking sonars, which can

obtain data regardless of thickness. We will examine the validity of our data in detail in the next section.

2.2 Ice sampling and analysis

Young ice and first-year ice samples were collected with sticks and a rope reinforced with wire, and their physical and chemical properties were examined. (Here, we use the term 'Young ice' and 'First-year ice' for the ice floe with thickness less than and greater than 30cm, respectively, regardless of growth processes.) They were kept in the ship's cold room (-15°C) during the cruise, and immediately after the cruises, they were carried into the ILTS cold temperature laboratory and kept at -16°C until ready for thin sectioning. The sampling locations are shown in Figure 3. The sampling area covers a relatively large region and the result of the analysis can be considered as representative of sea ice in the southern Sea of Okhotsk. However, it should be noted that sampling was biased to thinner ice due to the difficulty in picking up of thick ice samples.

To examine the ice growth processes, vertical sections were analyzed. Details of this analysis are described in *Ukita et al.* [2000]. Briefly, we first made a thick section of 5-mm thickness on glass plates to see the inclusions such as bubbles and brine pockets. Then we planed off the thick section to create a thin section of about 0.5-mm thickness, to observe the crystallographic structure by illuminating the ice sample between crossed-polarizers. Photographs of these thick/thin sections allowed us to examine textural variability. In determining the boundary of layered structures, the crystal arrangement shown in the thin section photographs was principally used. However, thick section photographs were also referred to when the distinction was vague. In counting the number of layers, if a columnar structure is recognized to have originated from the adjacent granular ice, these granular ice and columnar ice are regarded as one layer. The purpose of distinguishing ice layers here is to

examine how many ice floes have accumulated to make each ice sample. Columnar ice develops through thermodynamic bottom freezing, but sometimes the columnar ice extends upwards from granular ice. This is probably because the upper ice floe turned upside down as it rafted on top of the lower ice floe. In most cases, this structure can be discriminated through crystallographic observations. One example is shown in Figure 4 to explain our analysis. In this figure, three columnar layers are found with granular layers sandwiched between them. This figure clearly shows that several ice floes piled on each other to make up this ice sample. Granular structure can further be divided from the difference of grain sizes. From this figure, this ice sample appears to be composed of six layers. In the similar way, all the ice samples were analyzed and then the mean ice layer thickness (H_L in Table 3) by dividing the total ice thickness by the total number of layers.

Granular structure can be formed by either frazil ice accumulation or snow ice formation, and the layers produced through these two processes should be separately counted to examine the growth processes. Since it is often difficult to discriminate frazil ice from snow ice only through the observation of crystal texture, we used the isotopic composition data (^{18}O). Because snow generally has a much lower value of ^{18}O than sea water, the isotopic data make it much easier to discriminate the two kinds of ice. (From our analysis, the mean ^{18}O values of snow and seawater were about –15‰ and –1‰ respectively in this region.) For this analysis, we cut out a column with the basal area of 5cm x 6cm from each ice sample, and then sliced it into rectangular sections by cutting the columns vertically at the interval of 2cm. The number of sections amounted to 363 (first-year ice) and 359 (young ice). After melting the sections at a room temperature (about 20), we determined the isotopic compositions by averaging the results of twice measurements with a mass spectrometer (DELTA plus) for each sample. The analytical precision is estimated to be 0.02‰ from the root mean square of the twice measurements. The layers that were regarded as snow ice through this analysis are

excluded from the calculation of the mean layer thickness (H_L) in Table 3.

3. Results

3.1 Ice thickness distribution

The observation periods, the total number of observations and mean values of ice thickness is listed in Table 2. Sea ice begins to cover the southern Sea of Okhotsk in late January and reaches a maximum at the end of February. Therefore, all observation periods correspond to the ice growing season. The mean values of ice thickness varied considerably, from 18.5± 6.5 (*s.d.*) cm (1996) to 54.9± 22.9 cm (1997). The average ice thickness during 1991-2000 is 32.7± 9.9 cm (Table 2).

Prior to the main subject, it may be worth mentioning the relation between the thickness and extent of sea ice in this region. From the viewpoint of sea ice extent, our observation period from 1991 through 2000 is part of a three-decade period of less ice extent in the Sea of Okhotsk, though it has recovered to nearly normal since 1998 [*Japan Meteorological Agency*, 2000]. According to the analysis by the Japan Meteorological Agency, whereas the averaged sea ice area on February 10 in the southern Sea of Okhotsk (Lat.< 50°N) is 19.26 x 10^4 km^2 from 1971 to 2000, it is 17.28 x 10^4 km^2 from 1991 through 2000. The yearly values from 1991 through 2000 are 9.65, 18.93, 13.06, 16.68, 13.66, 18.22, 18.65, 22.32, 20.55, and 21.11 x 10^4 km^2 [Sapporo District Meteorological Observatory, personal communication, 2001] and show a slightly increasing trend during this decade. However, the mean ice thickness values do not have such a trend (Table 2) and seem to have no significant correlation with the sea ice area data (correlation coefficient = -0.21). This is probably because complex processes are involved in determining the ice thickness distribution, whereas the advance of the ice cover and thus its area/extent is primarily controlled by the wind field in the Sea of Okhotsk

[*Kimura and Wakatsuchi,* 1999]. In addition, as suggested by *Worby et al.* [1996] for Antarctic sea ice, the portion of ridged ice, which could not be counted in our analysis, may make a significant contribution to the total ice volume. To discuss the annual variation of ice thickness and volume in association with climatology, further ice thickness monitoring is required.

The time series of measured ice thickness data are plotted as an example with a 10-minutes (corresponding to a few kilometers) running mean line in Figure 5. This figure shows that although ice thickness varies considerably on a small time scale, a 10-minutes running mean seems to give the general trend of ice thickness. This is probably because the small-scale variations occur within one ice floe and about a few kilometers scale contains a number of ice floes. Here we regarded the values averaged over 10 minutes as the representative ice thickness for that region of the ice cover and mapped the ice thickness distribution along the ship track as shown in Figure 6. The geographical features of ice thickness in the southern Sea of Okhotsk are different from year to year. In 1997 and 1999, the ice was thicker in the eastern region than in the western region. In the thick ice region, the average thickness was more than 80 cm. On the other hand, the difference is not that much in the other years. Here we show the two typical examples of 1997 and 1998 in Figure 6. As processes controlling the ice thickness distribution, the wind field and the ice conditions at the time when ice cover spreads southward from off Sakhalin can be considered to be significant. They may not necessarily be relevant to sea ice area but cause a significant interannual variation of ice thickness distribution.

The ice thickness histogram in each year is shown in Figure 7. The thick end of each thickness distribution (here, defined as the ice thicker than the modal thickness) shows a nearly exponential decrease, as *Shimoda et al.* [1996] reported on the basis of the 1991 to 1994 data. In the next section, we try to explain the shape of the ice thickness distribution

using a simple rafting model.

Validity of ice thickness data

Prior to the discussion of the ice thickness distribution, we discuss the validity of our measurement method. For our data to be representative of the real ice thickness distribution, it is required (1) that ice floes were evenly broken and turned on to their sides in the same way regardless of ice thickness and (2) that the samples selected for measurement were free from subjectivity. Although it is quite difficult to examine these points exactly, we check the data validity by two ways of comparisons. For the first way, we compare our results with those obtained with an ice-profiling sonar. For the second way, we examine how much difference would be caused in the ice thickness distribution by different observers.

During winter 1999, ice draft was monitored using an ice-profiling sonar (upward-looking sonar) off Yubetsu, Hokkaido Island, (see Figure 1; *Fukamachi et al.* [2003]). Through this observation, a time series of ice draft data were obtained with an accuracy of about 10cm. With concurrent ice velocity data by ADCP, the thickness data were rearranged as a function of the spatial displacement of the ice. If we take as long a distance as the scale of the southern Sea of Okhotsk (~ a few hundreds of kilometers), the statistics of these data are assumed to be representative of the ice thickness distribution in the southern Sea of Okhotsk. It is considered that ice arriving at this location has traveled a long distance over a broad area. Thus, in spite of being a single point observation, the sonar data allow us to examine the validity of our measurement. The difference between ice thickness and draft is neglected here because the ice is relatively thin and thus the difference is almost the same order as the measurement error (about 10 cm). The period of 10 to 14 of February in 1999 is chosen for the comparison because it is the closest to our observation period among the available data. During this period, the total ice displacement was 106 km and the maximum ice drafts amounted to 5.22 m. Ice

thicker than one meter was excluded from the analysis because such thick ice is probably formed by ridging and beyond our measurement. The ice thickness distribution from sonar data is shown together with our result in Figure 7h. The figure indicates that the results from these two methods match well with the maximum difference being 6.0%, and the root mean square being 2.6%.

For very thin ice, broken ice would be finger-rafted more frequently rather than turned into side-up positions. Thus, although the minimum ice thickness that can be determined by this method is a few centimeters, our method may underestimate the frequency of very thin ice. From the visual observation, which was conducted during our cruise at hourly intervals, the averaged area occupied by nilas ranges from 5 to 15%. These values are a little higher than the frequencies at Hi=10cm in Figure 7. This underestimation for very thin ice is found also in the comparison with Yubetsu's data (Figure 7h). However, the difference is relatively small, and we do not consider that this underestimation alters our result substantially.

For the second way of comparison, we prepared two video cameras for ice thickness measurement during the cruise in February 2000. One was installed at the port side of the ship deck by NMRI and the other at the starboard side by ILTS. After the cruise, both organizations analyzed the video images independently. The two ice thickness distributions that were obtained are shown in Figure 7i. In spite of almost 100% difference in the number of samples, both distributions match within only a few percent at most near the peak (Figure 7i) and the average values of ice thickness are almost the same (see Table 2). In addition, the geographical ice thickness distributions are confirmed to be nearly the same (not shown). These results indicate that our method of ice thickness measurement is almost free from the observer's subjectivity. In brief, we consider that the ice thickness probabilities obtained by the video monitoring method are representative of the ice thickness distribution.

3.2 Ice texture and stratigraphy

First of all, we show the stratigraphy of all the 14 first-year ice samples (ice thickness larger than 30cm) in Figure 8 to describe the general features of the thicker ice. Each sample has quite variable vertical structure, indicating complex growth and thickening processes. Even so, we can find two common features in all the samples: (1) that granular ice occupies a significant part of the total volume, and (2) that most of the samples are composed of a number of relatively thin layers. The results of the whole ice samples, including young ice, are summarized in Table 3, which shows that the same textural/stratigraphic characteristics occur also in young ice samples. In the next subsection, we will examine these two characteristics in detail.

3.2.1 Granular structure

Concerning the first characteristics, six of the 14 first-year ice samples are composed entirely of granular ice (Figure 8). Also for young ice in 1996, all the layers were composed of granular ice. When sea water freezes, columnar ice is a result of thermodynamic congelation growth and can be clearly discriminated from granular ice. Thus it is shown that the bottom freezing is not so significant to the growth processes in this region.

On the other hand, granular ice is formed through either the accumulation of frazil ice under the turbulent conditions of swell and strong winds or snow ice formation due to the penetration of seawater into the snow layer on top of ice. As described in the previous section, ^{18}O was used here to discriminate these two types of ice. We measured ^{18}O of each 2cm-thick ice section, and then examined the corresponding crystal structure. The frequency distributions are shown separately for granular ice and columnar ice in Figure 9. It is noticed from this figure that both these two graphs, having prominent peaks around 0.80‰, are rather similar and that almost all the columnar ice sections take positive ^{18}O. The shift of the peak

to positive values is caused by isotopic fractionation during the freezing of seawater. Since columnar ice undoubtedly originates from sea water, these results suggest that there exists little difference of ^{18}O distribution between frazil and congelation ice, and that the negative values, found in granular ice, are attributed mostly to snow ice, affected by meteoric snow. Therefore, it seems to be reasonable to take ^{18}O<0 as an index for discriminating snow ice from frazil ice. This index is the same as that used for the Antarctic sea ice to discriminate snow ice by *Lange et al.* [1990] and *Jeffries et al.* [1997]. We counted the number of the ice sections which have negative ^{18}O, and calculated the ratio to the total number. According to this method, the snow ice fraction is estimated to be 12.1% (44 to 363) for first-year ice, 8.4% (30 to 359) for young ice, and 10.2% (74 to 722) for all the ice. Slightly higher fraction for first-year ice is probably because first-year ice spends longer time to grow in general and is exposed to snow effect for a longer period than young ice. The contribution of snow to the total ice thickness can be assessed based on two different criteria. One is the fraction of snow ice, and the other is the fraction of meteoric snow. *Ukita et al.* [2000] estimated meteoric snow fraction to be 8.5% from the ^{18}O analysis of the Okhotsk sea ice samples obtained mainly in 1996. According to their result, snow ice fraction is expected to be much greater than our estimation (=10%). (They did not estimate the snow ice fraction.) The discrepancy between our estimation and theirs can be attributed mainly to the treatment of a fractionation coefficient. They used the value of 2.7‰ as a fractionation coefficient. However, we consider that it should be lower than this value in the light of the fact that the difference of ^{18}O between the surface Okhotsk sea water (mean: -1.01‰) and ice samples (mode: about 0.80‰) is much smaller than 2.7‰ If they used 1.81‰ (=0.80+1.01) as a fractionation factor, the meteoric snow fraction would be reduced to 1%. Considering the fact that the snow ice fraction is by several times larger than the meteoric snow fraction for the Antarctic sea ice (*e.g. Lange et al.* [1990], *Jeffries et al.* [1994], and *Jeffries et al.* [1997]), our estimation would be

probable. We therefore conclude that granular ice (74%) is composed of frazil ice (64%) and snow ice (10%), indicating that frazil ice is still the most dominant in this area.

In brief, the above results indicate that a turbulent process such as frazil ice accumulation is much more significant in the southern Sea of Okhotsk than either thermodynamic congelation growth or snow ice formation. This is consistent with the estimate of heat budget by *Toyota et al.* [2000] and *Ohshima et al.* [2003] in that congelation growth is limited and does not play an important role in growth processes even in mid winter in this region. In our first-year ice samples, the thickness of columnar ice ranged from 1 to 34 cm, and the average was 7.8cm, corresponding to only 17 % of the mean ice thickness (45cm). It is considered that the accumulation and solidification processes of frazil ice, which were investigated from laboratory experiments by *Martin and Kauffman* [1981], occur frequently in this region.

Fractions of columnar and granular ice have been investigated from the analysis of ice samples in both polar regions. For the Arctic, the dominance of columnar ice relative to granular ice has been reported. For example, *Gow et al.* [1987] estimated that columnar ice accounts for more than 75% of the sea ice in the Fram Strait, and *Eicken et al.* [1995] estimated that columnar/frazil ice accounts for 61/18% of the undeformed sea ice in the Eurasian sector of the Arctic Ocean. On the other hand, for the Antarctic it has been reported that granular ice of frazil origin dominates over columnar ice. For example, *Lange and Eicken* [1991] showed that granular ice of frazil origin occupies 50 to 70% fraction in the Weddell Sea. *Jeffries and Adolphs* [1997] reported that the fraction of columnar ice is only 22% in the Ross Sea in the outer pack ice >800km from the coast. *Jeffries et al.* [1997] estimated frazil/columnar as 44/26% for sea ice in the Bellingshausen and Amundsen Seas. *Allison and Worby* [1994] showed that approximately 50% is composed of small frazil crystals off East Antarctica.

This difference between the Arctic and the Antarctic regions can be explained as follows:

the Antarctic ice cover is less geographically constrained than in the Arctic Ocean, and the resulting more divergent ice cover has a higher proportion of open water where frazil ice growth is promoted in the wind- and wave- affected environment. The result of our structural analysis is closer to that of the Antarctic regions, and it is likely that granular ice formation also occurs in the Sea of Okhotsk where it is windy and ice floes are highly mobile due to the lack of geographical constraint.

3.2.2 Layered structure

Next, we examine the second feature found in Figure 8, that most of the samples are composed of a number of thin layers. Above all, snow ice layers are found much below the surface in some samples, indicating the evidence of piling-up processes. Table 3 shows that, on the average, ice floes of 5 to 10 cm thick pile up on each other and thereby make up one composite ice slab. For dynamic thickening processes, rafting seems to be more important than ridging when ice is thin. For example, *Worby et al.* [1996] reported from wintertime ship-based visual observations in the Antarctic ice cover that ridging is not as common as rafting when the ice thickness is less than 60 cm. Since most of the sea ice floes are less than 60 cm (see Figure 7) in our case, rafting is probably more important than ridging. This is also confirmed by visual observations during the cruise.

The importance of the rafting process has been pointed out in the Antarctic from ice structure analysis [*e.g. Lange et al.*, 1989; *Lange and Eicken*, 1991; *Worby et al.*, 1996; *Jeffries and Adolphs*, 1997; *Jeffries et al.*, 1997]. *Worby et al*. [1996] have estimated the average thickness of the individual layer for the ice in the Bellingshausen and Amundsen Seas to be only 12 cm. *Jeffries and Adolphs* [1997] estimated it for the western Ross sea ice to be 20 cm for the inner pack ice and 12 cm for the outer pack ice. Based on observational results, *Lange et al*. [1989] proposed a conceptual model named the '*pancake cycle*' as a thickening

process by piling-up. Their model is as follows: pancake ice floes initially form in the open ocean; these floes pile up partly on each other due to the strong wind and swell; water appears between the rafted pancakes; further pancake ice floes form in this open area and continue to pile on each other. The repetition of this process enables the sea ice to be thickened. In the case of the Sea of Okhotsk, however, such turbulent conditions have not occurred in the pancake ice fields during our cruises as far as we know from visual observations. This is probably because oceanic conditions are not so turbulent in this area as in the Antarctic, and thus the piling-up process does not seem to be so vigorous as in the Antarctic. Figure 10 shows the typical sea ice area in this region. It is noted in this figure that some part of ice floes overlaps (See the whitish area.), indicating that a rafting process is occurring. This is the process that we are considering here. Although the situation shown in Figure 10 seems to be rather closer to a regular rafting than the '*pancake cycle*' proposed by *Lange et al.* [1989], we consider that the concept is analogous in that open water area is produced by piling-up of ice floes and the accumulation of ice floes is important in ice thickening process. Hereafter we call it '*rafting cycle*' in this paper.

4. Ice growth model

In this section, on the basis of the observational results shown in the previous section, we propose a simple rafting cycle model and provide insights into the ice thickening process in the Sea of Okhotsk.

4.1 Model concept

We begin by examining the observational result that the ice thickness distribution decreases exponentially for the thick ice end. Mathematically, an exponential decrease of

probability implies that the ratio of the neighboring bins is constant. When ΔH denotes bin width,

$$\frac{P_{i+1}}{P_i} = \frac{P(h_{i+1})}{P(h_i)} = \frac{e^{-a(h_i + \Delta H)}}{e^{-ah_i}} = e^{-a\Delta H} = const. \quad , \tag{1}$$

where P_i denotes the probability of ice with the thickness of $i \times \Delta H$. In our case, this means that the areal fraction of $h_{i+1}(=h_i + \Delta H)$ thick ice to h_i thick ice is always constant. If we assume that h_{i+1} thick ice is produced merely by the piling-up of ΔH thick ice on h_i thick ice, then the areal fraction of h_i thick ice on which ΔH ice is piled up is constant, regardless of ice thickness. In other words, it can be said that during a rafting event a unit ice floe ΔH thick piles up on the ice floe of each thickness category in proportion to its area. Here, it is assumed that ice formation makes a unit ice floe of ΔH thick only over open water. This assumption seems to be reasonable when we take it into account that congelation ice growth is estimated to be small [*Toyota et al.,* 2000] and the ice production occurs mostly in thin ice and open water area [*Ohshima et al.*, 2003]. Our concept of the ice thickening process is summarized as follows. In the first place, sea ice floes of ΔH thick form over open water. When a rafting event, probably induced by a strong winds or waves/swell, occurs, these unit ice floes pile up on others at a constant areal ratio (p) of the sea ice area, resulting in the production of sea ice of $2\Delta H$ thick. Then, sea ice forms again over the open area created by rafting. The repetition of the same process makes sea ice thicken step by step. This concept implies that the repetition of the ice formation over the open water and the sequential piling-up process is important in the thickening process. In addition, this model is also consistent with our sea ice structural features that indicate that dynamic processes are important since most of the ice samples are composed of a number of thin layers.

Next, let us examine this process quantitatively in an analytical way. Figure 11 is a schematic picture for explaining this concept. Time step corresponds to a rafting event. Initially (*time step 0*), the area is covered with an ice floe of H thick. The areal fraction is 1 for H thick ice, and zero for ice of other thickness. At time step 1, the areal fraction *p* is rafted to produce the ice area of 2 H thick and is replaced by open water. Then the open water area is covered again by newly formed ice before the next time step. Thus, the areal fraction becomes *1-p* for H thick ice, *p* for 2 H thick ice, and 0 for ice of other thickness. At time step 2, 3 H thick ice is generated by the rafting of H ice on the fraction *p* of 2 H thick ice area. The areal fraction of 3 H thick ice is calculated to be p^2 [$=p$ p]. At the same time the fraction *p* of H thick ice area is also used to generate 2 H thick ice again and the fraction of 2 H thick ice is calculated to be *2p(1-p)* [$=p-p^2+p(1-p)$]. The fraction of H thick ice is calculated as *(1-p)²* [$=1-p^2-2p(1-p)$] as a residual area. Before time step 3, the open area created by rafting is covered again by newly formed ice. Similarly, at time step 3 the fractions of 1,2,3,4× H thick ice are calculated as *(1-p)³, 3p(1-p)², 3p²(1-p), p³*, respectively. The evolution of thickness distribution is summarized in Table 4. Through the repetition of this process, the maximum ice thickness increases. According to this scenario, the areal fraction of m H thick ice (P_m) at the time step *n* can be described in a general manner as

$$P_m = {}_nC_{m-1} \cdot p^n \cdot (1-p)^{n-m+1} \qquad (2)$$

This formula yields the ice thickness distribution at time step n, if *p* is provided. It is noted that this formula is exactly equal to the Binomial Distribution. Namely, it shows that the thickness distribution determined by our concept can be expressed as the probability of occurrence of piling-up if rafting events occur *n* times randomly with the probability *p*. This expression can be regarded as a simplified formulation of a rafting process if it occurs simply

in a stochastic process independent of ice thickness.

4.2 Validation of model

From direct observation of the rafting phenomenon, it is not easy to show that the real rafting process can be expressed by this simplified stochastic model. In this paper we make an attempt to validate our model by comparing the ice thickness distribution calculated from (2) with the observational results. However, it is almost impossible to count the number of rafting events (n) and to estimate the piling-up ratio (p) at one rafting event. Thus, (2) can hardly be validated from the observations if we treat it in this style.

From a statistical viewpoint, it is generally known that the Binomial Distribution approaches the Poisson Distribution for large n and small p with the condition that n p is finite. In our case, this condition seems to be applicable because rafting events occur repeatedly and the piling-up ratio may not be so large. According to the Poisson Distribution, the ice thickness distribution (P_m) can be described as

$$P_m = \frac{\mu^{m-1}}{(m-1)!} \cdot e^{-\mu} \quad ,$$

(3)

where μ ($=np$) denotes the average of the Binomial Distribution. To put it explicitly, μ is the average number of piling-up events and is given as $H_{im}/$ H (H_{im} = mean ice thickness). For example, in the case of 1994, μ is 7.8, 3.9, and 2.6 for   H= 5, 10, and 15 cm, respectively (refer to Table 2 for H_{im}). It should be noted that (3) includes neither n nor p. This formulation makes the problem much easier. All we have to do to obtain the ice thickness distribution for model validation is to calculate the mean ice thickness and to give the thickness   H of a unit ice floe. In this case,   H is treated as a tuning parameter. In the

previous section, we discussed the feature of exponential decrease seen in the thickness histogram to get a hint associated with our rafting cycle model. Although the exponential decrease and the Poisson Distribution are different functions, this feature is seen only for the thick end, and thereby is not inconsistent with the Poisson Distribution described in this section.

We validate our conceptual model by examining whether the observed ice thickness distribution follows the Poisson Distribution expected from our model. Here, the Poisson Distribution is given by substituting μ, calculated from the assumed H and the averaged mean thickness H_{im} for each year, into (3). The results are summarized in Figure 12, where the vertical axes are scaled by the probability density function to compare with the Poisson Distributions for different H It can be seen that the observed ice thickness distributions fit the Poisson Distributions well in most years, particularly in 1992 and 1998.

On the other hand, slight disagreement can be seen for 1991 and 1999. For 1991, the measurements did not seem to be representative of the process discussed here because the data were taken only from the very limited region. For 1999, although the comparison for the total area shows disagreement, the ice thickness distribution for the western region (Lon.<144.5$^{\text{o}}$E), where relatively thin ice is dominant, agrees well with the Poisson Distribution for $H= 5$ cm (Figure 13a). Thus, the disagreement is caused primarily by the ice thickness distribution in the eastern region (Figure 13b). The difference of distributions between the western and eastern part may be attributed to the ice growth history. By tracing the daily change of ice concentration obtained from SSM/I data, it is revealed that highly concentrated ice area moved southward from off Sakhalin to the eastern part. This suggests that the sea ice in the eastern part originated mainly from the area off Sakhalin, while in-situ freezing is prominent in the western part. In the northern region, H is expected to have a much larger value because of lower air temperatures and the smaller amount of solar radiation.

As the sea ice moves to the south, H would become lower. In this case, the ice thickness distribution would have the mixed structure of the Poisson Distributions for different H, and the shape of the thickness distribution in Figure 13b does appear to have a somewhat complicated structure.

Figure 12 shows that the best fit H is 10cm in 1997. Here, we consider why H is thick (10 cm) in 1997 compared with other years (5 cm). In 1997, the mean ice thickness amounted to as much as 55 cm (Table 2) and columnar ice was prominent compared with other years (Table 3). Considering that the 1997 meteorological conditions in the southern Sea of Okhotsk were almost similar to those in all other years (Table 1), these results suggest that many thick ice floes, which grew mainly in the northern region, were advected southward and covered the study area in 1997. We consider that this growth history is responsible for the thicker H in 1997. Actually, the averaged layer thickness (9.7cm) was the thickest among the 5 years (Table 3). Probably because the southward spreading occurred in a relatively wide area in 1997, the total ice thickness distribution agreed well with the Poisson Distribution, unlike the case of 1999. In any case, the best fit thickness of 5 to 10 cm for H is consistent with the result of the ice structural analysis (Table 3), which supports our conceptual model of ice thickening processes. In brief, it is concluded that the observed ice thickness distributions match well with the Poisson Distribution.

Finally, we mention the strength of this model. The point is that we can obtain the ice thickness distribution from calculation easily if the ice growth amount in open water, and the number of rafting events are given. This model implies that the piling-up of nilas or young ice is essential to the thickening process of first-year ice in this region. In addition, since the rafting process of sea ice is not well understood, our model may provide the possible history regarding rafting events. However it has to be noticed that this rafting cycle model can be available only to the ice area where the thickness is thin and a rafting process is more

dominant than a ridging process. (For example, *Worby et al.* [1996] pointed out that ridging is more common for most ice floes with more than 60cm thickness in the Antarctic.)

4.3 Comparison with other models

The relationship between the ice thickness distribution and the ice thickening process has been discussed theoretically by some researchers [*Hibler et al.*, 1972; *Thorndike et al.*, 1975; *Thorndike*, 1992, 2000]. However, their studies are mainly intended for perennial ice regions, not seasonal ice zones where ice thickness is relatively thin. It does not seem to be meaningful to directly compare the result of our model with theirs. Therefore, in this paper we will examine our model by considering how it can be expressed in the formulation by *Thorndike et al.* [1975] which has been used in several numerical sea ice models [*e.g. Hibler*, 1980; *Flato and Hibler*, 1995]. This examination may serve to understand the concept of our model.

Combining the effects of advection, thermodynamical growth, and mechanical ridging, *Thorndike et al.* [1975] derived the following governing equation for the variation of the ice thickness distribution,

$$\frac{\partial g}{\partial t} = -div(g\boldsymbol{V}) - \frac{\partial (fg)}{\partial h} + \Phi \quad ,$$

where g(h), $\boldsymbol{V}$, and f (=dh/dt) are the probability density function of ice thickness, the ice velocity, and the thermodynamic growth rate, respectively. The last term   is a redistribution function and represents the mechanical thickening processes. The first term of the right-hand side represents divergence/convergence and does not seem to be essential because we now consider the whole area of the southern Sea of Okhotsk and the effect of much thicker ice floes from the north is still small in early February. The contribution of the

second term, *i.e.*, thermodynamic thickening by congelation ice growth, seems to be small except for open water. *Toyota et al.* [2000] showed from in-situ observation in this region that the ice growth rate, averaged over all the ice thickness, is estimated to be less than 1 cm/day, and more than half of the total ice growth amount is owed to open water and thin ice less than 10cm. Therefore, the second term is estimated to be less than $0.1\times$ g day^{-1} if we take 10cm for the bin width (Δh). This means that it takes more than 10 days to have g alter by just one. On the other hand, the third term easily alters g by just one rafting event. Therefore, it seems to be the third term that essentially determines the ice thickness distribution in this region at this season of the year. *Thorndike et al.* [1975] described as

$$= [-a(h)+n(h)] \; div \; \textbf{\textit{V}} ,$$

where a(h) denotes the thickness distribution of the ice participating in the ridging /rafting, and n(h) is that of the newly ridged/rafted ice. In their case, a(h) is assumed to be b(h) g(h), where b(h) is introduced to enhance a(h) when h is small. In other words, it represents the effect that thinner ice is easier to become involved in ridging/rafting. The term n(h) is expressed as a function of a(h) under some assumptions related to the way the ice is ridged/rafted. In their case, they assumed that the ice thickness becomes five times thicker than the original ice floe during one ridging event. In the polar ice pack region, ridging events possibly occur more frequently than rafting events because the newly formed ice floes are much thinner than the surrounding perennial ice floes. On the other hand, in our case rafting events seem to be more frequent than ridging events because the ice is thin and the difference of thickness between newly formed ice and the surrounding ice is relatively small. Thus n(h) is produced by the rafting of unit ice floe on the ice of h- H thickness. Consequently, in our model a(h) and n(h) are expressed as p g(h) and p g(h- H), respectively. Therefore, close

comparison shows that *p* in our model corresponds to b(h) div **V** t in the *Thorndike et al.* [1975] model, where t is the duration of the rafting event. This implies that the likelihood of ridging (or rafting) does not depend on ice thickness in our model when *div **V*** and t are given. Here we show the result of our model for the case of *n* (number of rafting events) =24 and *p* (piling-up ratio) =0.2. The calculated distribution is shown with a thick solid line in Figure 14a, and the graphs of -a(h) and n(h) in our model are also shown with broken lines in Figure 14b. It is noticed in Figure 14a that the calculated thickness distribution almost follows the Poisson Distribution. It can be seen from Figure 14b that the fraction of the ice participating in ridging is larger for thinner ice and that the sum (= -a(h)+n(h)) is negative for thin ice and positive for thick ice. This feature is similar to the *Thorndike et al.* [1975] model (see their Figure 7). Therefore, it can be said that our model is a similar version of the formulation by *Thorndike et al.* [1975].

4.4 Tuning parameter

Now we shall look more carefully into the tuning parameter Ḥ a unit ice thickness. In most cases a thickness of 5 cm yielded the best fit to the Poisson Distribution as H Also, from the ice structure data it was shown that sea ice thickens by the piling-up of 5 to 10 cm thick ice floes. Here we examine whether the value of 5 cm is reasonable as a unit ice thickness from the thermodynamic point of view. For this purpose, we estimate the amount of thermodynamic ice formation over open area during the period between rafting events. Generally there are two types of ice growing. One is a congelation growth (nilas-type) and the other is frazil ice formation in sustained open water. Here we examine both types of growth. Before the calculation, we need to examine how frequently the main rafting events occur. As an example, we show the time series of wind speed in 1995/1996 winter (Figure 15). The arrows represent the local maxima of wind speed in January and February, and 19 arrows are

found during the two months, indicating that local maxima occur about every three days. This feature has been observed during this season in other years. Since strong winds are considered to be a key factor in the occurrence of rafting events, we assume that the arrows in Figure 15 indicate rafting events. Therefore, we calculate the typical thermodynamic ice growth amount for three days. For the representative estimation, we obtain the daily mean meteorological data for about one week and then examine the ice growth amount for three days under the typical meteorological conditions. Here, we adopt the average during the last 11 days of January, 1996, which corresponds to the period just before our observations.

For a congelation ice case, we calculated the ice growth amount for three days under the same conditions, using a one-dimensional (vertical) thermodynamical model which is basically the same as that used in Maykut [1978]. The main differences are (1) that *Maykut* [1978] used the ice thickness distribution calculated from Thorndike's model, while thickness is unique in our case and (2) that the incoming long wave radiation is fixed in Maykut's case, while the calculated value from the empirical formula by *Maykut and Church* [1973] is given in our case. No snow on sea ice is assumed. Ocean heat flux is neglected here. The method of calculating the ice growth amount is the same. (see *Toyota and Wakatsuchi* [2001] for details).

For meteorological data we use ECMWF twice daily gridded air temperature, wind, and relative humidity. Cloud amount is assumed to be 7/10 on the basis of in-situ observations (see Table 1). For daily solar radiation (Q_s), the empirical formula (Q_{s0}) developed by *Kim and Kimura* [1995] for the ocean adjacent to Japan is modified here, taking into account the effect of optical multiple reflection by snow and ice. Q_s is described as follows

$$Q_s = 1.325 \, Q_{s0} - 7.2697$$

$$Q_{s0} = I_0 \, (0.865 - 0.5 \, C^2)$$

where C is cloud amount in tenths and I_0 is the solar radiation over the sea surface in the absence of cloud as suggested by *Seckle and Beaudary* [1973]. A formula to convert Q_{s0} to Q_s is obtained from the regression between the calculated Q_{s0} and the observed solar radiation at four meteorological observatories near the coast of Hokkaido, Japan. The distribution of the calculated ice growth rate averaged for the initial three days is depicted in Figure 16a for the wide area of the Sea of Okhotsk. In this figure, the region used for calculation is limited to the sea ice area during the last 11 days of January, which was determined from the daily images of the Special Sensor Microwave/Imager. The ice growth rate in our study area is about 2 cm/day, corresponding to the growth amount of about 6cm for three days. This value almost coincides with both the observed average thickness of columnar ice (7.9cm) and the unit floe thickness assumed in our model (5 to 10cm). In addition, it is noted that it amounts to 3 to 4 cm east of Sakhalin (50°N), corresponding to about 10 cm for three days. This value coincides with the unit floe thickness in 1997 and supports our earlier speculation on the ice growth history in 1997. In this calculation, we assumed only the congelation ice growth.

For a frazil ice case, it is difficult to predict the growth rate because it also depends on the swell and wind conditions. Here, we estimate the growth amount by calculating the heat flux taken away from the open water surface. Although this may not be the exact estimation of granular ice thickness, it seems to be useful to examine the order of thickness. The result is shown in Figure 16b. From this figure the growth rate in our study area is estimated again as about 2cm/day, corresponding to about 6 cm for three days. From observation, the mean layer thickness of frazil ice, which is calculated by excluding snow ice layers from granular ice layer, is estimated as 7.0 cm. Thus the estimated value coincides with both the ice texture analysis and the unit floe thickness in our model. Consequently, this result suggests that 5 to 10 cm thick is reasonable as a unit ice floe thickness.

5. Summary and Discussion

On the basis of in-situ observations, the thickness distribution and structure of the sea ice in the southern Sea of Okhotsk have been described, and on the basis of these data, a simple conceptual model for ice thickening in the southern Sea of Okhotsk has been proposed. The ice thickness data were obtained quantitatively with a video monitoring system each winter from 1991 to 2000 except 1995. Concurrently, 14 first-year ice and 33 young ice samples were collected during the cruises from 1996 to 2000 to examine the ice structure. From the ice thickness data analysis, it is shown that the averaged ice thickness ranges from 19 ± 7 to 55 ± 23 cm and that the thickness distribution decreases exponentially at the thick end, and the entire distribution follows a Poisson Distribution as a whole. It is shown from ice structure analysis that granular ice occupies 74% of the total thickness of ice sampled, and that ice samples are composed of several layers of 5 to 10 cm thick on average. In addition, the snow ice fraction is estimated to be about 10% of the total thickness from the analysis of isotopic compositions, indicating that the frazil ice fraction occupies 64% of the total thickness and are still much more than that of columnar ice. These results suggest that the frazil ice formation and piling-up processes are much more important than a congelation process in this area.

It is shown that these observational features can be explained to some extent by the following simple rafting cycle model. That is, sea ice floes are first formed over open water, and then a portion of the ice floes piles up on the surrounding ice floes during a rafting event. Over the open water produced by rafting, sea ice is again formed. At the next rafting event, ice floes formed over open water area pile up on the surrounding ice in proportion to the area of each thickness category. This concept is analogous to the *pancake cycle*, which is considered a common ice thickening process for Antarctic sea ice, in that the repetition of the

ice formation over the open water and the sequential piling-up process is important in the thickening process.

Our model is based on some assumptions. First, we assume that the piling-up ratio p is constant. As mentioned before, this assumption implies that the likelihood of rafting does not depend on the thickness of the ice floes on which unit ice floes are piled up if any kind of sea ice has the same chance to meet with unit ice floes. As sea ice thickens, rafting would become more difficult and thus this assumption would be broken. Therefore we consider that this assumption can be applied only to thin ice areas like the southern Sea of Okhotsk. Nevertheless, p is also relevant to $div\ \boldsymbol{V}$, and thus may not be necessarily constant. Actually, the divergence of wind varies by several times in this region. In order to examine to what extent the variation of p at each rafting event affects our result, we conducted three cases of the calculation of ice thickness distribution for $n=24$, where we provided various p at each rafting event with keeping the average of p being 0.2. In the first case, we provided p with 0.2 (constant) for all the rafting events. In the second case, we provided p with 0.1 for $1 \leq n \leq 8$, 0.2 for $9 \leq n \leq 16$, and 0.3 for $17 \leq n \leq 24$. In the third case, we provided p with 0.05 for $1 \leq n \leq 4$, 0.10 for $5 \leq n \leq 8$, 0.15 for $9 \leq n \leq 12$, 0.25 for $13 \leq n \leq 16$, 0.30 for $17 \leq n \leq 20$, and 0.35 for $21 \leq n \leq 24$. For these three cases, it should be noticed that the averages of p are all 0.20. The results are shown in Figure 14a. The first case is drawn with a thick solid line, and the second and third cases are drawn with broken lines. The difference among these results is quite small and can hardly be detected. This result shows that the variation of p at each rafting event does not alter our result substantially, and therefore the ice thickness distribution can be calculated with accuracy if we know the representative p. In the future, the value of p should be determined through either laboratory experiments or observation.

Second, we assume that the unit ice floes that are involved in piling-up are only from H thick ice. Of course, it should be possible that the ice floes with the thickness of more than

H are involved in piling-up. Since the piling-up between thicker ice floes would be able to thicken sea ice more effectively than our scenario, the probability of thick ice should be significantly larger than the Poisson Distribution based on our assumption if this process occurs frequently. However, Figures 12 and 13 do not show such a trend. We consider that this is because when the ice floes with the thickness of more than H are involved in piling-up, ridging is more likely to occur than rafting and these ridged ice floes are not counted in our measurement. The likelihood of rafting and ridging has recently been examined through numerical simulations by *Hopkins et al.* [1999]. They considered the process of rafting and ridging between two identical sheets which consists of thin (30%) and thick (70%) sea ice. According to their result, in the rafting portion the number of accumulated ice floes is two or three while more than five ice floes contribute to the ridging portion; thus, the rafting and ridging portions are clearly discriminated (see their Figure 6,7,8). From their result, it is inferred that although the ice floes with the thickness of more than H participate in piling-up, they contribute mainly to the ridging process, not to the rafting process. This may support our speculation because in our analysis the ridged ice were excluded and mainly the rafted ice were counted.

Despite its importance, as *Hopkins et al.* [1999] pointed out, rafting has not drawn as much attention as pressure ridging. Given that rafting events frequently occur under the turbulent conditions and affect the ice thickness distribution significantly in the vast MIZ, it is essential to understand the rafting mechanism. Both observational and theoretical studies are required. Further observations of the ice thickness in MIZ are also required. As a final goal, the rafting process needs to be better parameterized in numerical sea ice models aimed at understanding climate systems. We hope that this paper is a step toward this goal.

Acknowledgements

Reference list

Allison, I., and A.P. Worby, Seasonal changes in sea ice characteristics off east
Antarctica. *Ann. Glaciol.*, 20, 195-201, 1994.

Eicken, H., M. Lensu, M. Lepparanta, W.B. Tucker III, A.J. Gow, and O. Salmela,
Thickness, structure, and properties of level summer multiyear ice
in the Eurasian sector of the Arctic Ocean, *J. Geophys. Res.*, 100,
22,697-22,710,1995.

Flato, G.M. and W.D. Hibler, Ridging and strength in modeling the thickness
Distribution of Arctic sea ice, *J.Geophys.Res.*,100,18,611-18,626,1995.

Fukamachi, Y., G.Mizuta, K.I.Ohshima, H.Melling, D.Fissel, and M.Wakatsuchi,
Variability of sea-ice draft off Hokkaido in the Sea of Okhotsk revealed by a
moored ice profiling sonar in winter of 1999, *Geophys.Res.Lett.*, 30(7), 1376, doi:
10.1029/2002GL016197, 2003.

Gow, A.J., W.B. Tucker III, and W.F. Weeks, Physical properties of summer sea ice
in the Fram Strait, June-July, 1984, *CRREL Report,* 87-16, 81pp, 1987.

Hibler, W.D., W.F. Weeks, and S.J. Mock, Statistical aspects of sea-ice ridge
distribution, *J. Geophys. Res.*, 77, 5954-5970, 1972.

Hibler, W.D., Modeling a variable thickness sea ice cover, *Mon. Weather Rev.*, 108,
1943-1973, 1980.

Hopkins, M.A., Rafting and ridging of thin ice sheets, *J. Geophys. Res.*, 104,
13,605-13,613, 1999.

Japan Meteorological Agency, The statistical data of sea ice, No.3, CD-ROM,
Tokyo, Japan, 2001.

Japan Meteorological Agency, The results of sea ice observations, 18, 45pp.,
Tokyo, Japan, 2000. *(in Japanese)*

Jeffries, M.O., R.A.Shaw, K.Morris, A.L.Veazey, and H.R.Krouse, Crystal structure,

   stable isotopes (18O), and development of sea ice in the Ross, Amundsen, and

   Bellingshausen seas, Antarctica, *J.Geophys.Res.*, 99, 985-995, 1994.

Jeffries, M.O., and U. Adolphs, Early winter ice and snow thickness distribution,

   ice structure and development of the western Ross Sea pack ice between the ice

   edge and the Ross Ice shelf, *Antarctic Sci.*, 9, 188-200, 1997.

Jeffries, M.O., A.P. Worby, K. Morris, W.F. Weeks, Seasonal variations in the

   properties and structural composition of sea ice and snow cover in the

   Bellingshausen and Amundsen Seas, Antarctica, *J. Glaciol.*, 43, 138-151, 1997.

Kim, Y.-S., and R.Kimura, Error evaluation of the bulk aerodynamic method for

   estimating heat flux over the sea. *J.Korean Meteor. Soc.*, 31, 399-413, 1995

Kimura, N., and M. Wakatsuchi, Processes controlling the advance and retreat of sea

   ice in the Sea of Okhotsk, *J. Geophys. Res.*, 104, 11,137-11,150, 1999.

Lange, M.A., S.F. Ackley, P. Wadhams, G.S. Dieckmann, and H. Eicken,

   Development of sea ice in the Weddell Sea, *Ann. Glaciol.*, 12, 92-96, 1989.

Lange, M.A., P. Schlosser, S.F. Ackley, P. Wadhams, and G.S. Dieckmann,

   J.Glaciol.,36,315-323,1990.

Lange, M.A., and H. Eicken, Textural characteristics of sea ice and the major

   mechanism of ice growth in the Weddell Sea, *Ann. Glaciol.*, 15, 210-215, 1991.

Martin, S. and P. Kauffman, A field and laboratory study of wave dumping by grease

   ice, *J.Glaciol.*,27,283-313,1981.

Maykut, G.A., and P.E. Church, Radiation climate of Barrow, Alaska, 1962-66.

   J. Appl. Met., 12, 620-628, 1973.

Maykut, G.A., Energy exchange over young sea ice in the central Arctic,

   J. Geophys. Res., 83, 3646-3658, 1978.

Ohshima, K.I., T. Watanabe, and S. Nihashi, Surface heat budget of the Sea of Okhotsk

    during 1987-2001 and the role of sea ice on it, *J. Meteor. Soc. Japan,* 81, 653-677, 2003.

Seckle, G.R. and F.H. Beaudry, The radiation from sun and sky over the North

    Pacific Ocean, *Trans. Amer. Geophys. Union*, 54, 1114, 1973.

Shimoda, H, S. Uto, K. Tamura, and H. Narita, Sea ice situations in the Sea of Okhotsk

    off the coast of Hokkaido by on board ship observations *(in Japanese)*,

    Proceedings of The eleventh international symposium on Okhotsk Sea

    and Sea Ice, Mombetsu, p156-160, 1996.

Shimoda, H., T. Endo, K. Muramoto, N. Ono, T. Takizawa, S. Ushio, T. Kawamura,

    K.I. Ohshima, Observations of sea-ice conditions in the Antarctic coastal region

    using ship-board video cameras *(in Japanese)*, *Antarctic Record*, 41,

    355-365, 1997.

Thorndike, A.S., D.A. Rothrock, G.A. Maykut, and R. Colony,

    The thickness distribution of sea ice. *J. Geophys. Res.*, 80, 4501-4513, 1975.

Thorndike, A.S., Estimation of sea ice thickness distribution using observations

    and theory, *J. Geophys. Res.*, 97, 12,601-12,605, 1992.

Thorndike, A.S., Sea ice thickness as a stochastic process, *J.Geophs.Res.*,105,

    1311-1313, 2000.

Toyota, T., J. Ukita, K.I. Ohshima, M. Wakatsuchi, and K. Muramoto,

    A measurement of sea ice albedo over the southwestern Okhotsk Sea,

    J. Meteor. Soc. Japan, 77, 117-133, 1999.

Toyota, T., T. Kawamura, and M. Wakatsuchi, Heat budget in the ice cover

    of the southern Okhotsk Sea derived from in-situ observations,

    J. Meteor. Soc. Japan, 78, 585-596, 2000.

Toyota, T and M. Wakatsuchi, Characteristics of the surface heat budget during the

Ice-growth season in the southern Sea of Okhotsk, *Ann.Glaciol.*, 33, 230-236.

Ukita, J., T. Kawamura, N. Tanaka, T. Toyota, and M. Wakatsuchi, Physical and stable isotopic properties and growth processes of sea ice collected in the southern Sea of Okhotsk, *J. Geophys. Res.*, 105, 22,083-22,093, 2000.

Wadhams, P., A.S. Mclaren, and R. Weintraub, Ice thickness distribution in Davis Strait in February from submarine sonar, *J. Geophys. Res.*, 90, 1069-1077, 1985.

Worby, A.P. and I. Allison, Ocean-atmosphere energy exchange over thin, variable concentration Antarctic pack ice, *Ann. Glaciol.*, 15, 184-190, 1991.

Worby, A.P., M.O. Jeffries, W.F. Weeks K. Morris, and R. Jana, The thickness distribution of sea ice and snow cover during late winter in the Bellingshausen and Amundsen Seas, Antarctica, *J. Geophys. Res.*, 101, 28,441-28,455, 1996.

Figure captions

Figure 1: Map of the southern Okhotsk Sea with the ship tracks for 1996-2000 with

the mean ice edges on February 10 for 1971 to 2000 (thick broken line).

The mean ice edges are adopted from the *Japan Meteorological Agency* (2001).

The triangle marks the location of ice thickness monitoring by upward-looking

sonar in 1999 winter. The water depth there is 58 m.

Figure 2: Ice thickness measurement by video monitoring.

Schematic diagram of observation technique (after *Shimoda et al.*, 1997).

Figure 3: Locations of young and first-year ice samples which were collected

from 1996 to 2000. The broken lines denote the mean ice edges on February 10

for 1971 to 2000. The numbers in bold correspond to the first-year ice samples

illustrated in Figure 8.

1: 96A, 2: 97A, 3: 97B, 4: 97C, 5: 97D, 6: 98A, 7: 98B, 8: 98C, 9: 99A

10: 99B, 99D 11: 99C, 12: 2000A, 13: 2000B.

Figure 4: Samples of thick (a) and thin (b) sections.

This is a sample of 40 cm thick ice taken in 1997, corresponding to 97A in Figure 8.

Note that columnar ice is sandwiched between granular ice at three locations,

suggesting the importance of a dynamic accumulation process. The arrows show

the boundaries of layers used for the calculation of H_L in Table 3.

The thick ice (5mm) structure revealed by the scattered light.

The thin section (< 1mm) illuminated between crossed polarizers.

Figure 5: Ice thickness data.

An example of time series of ice thickness data (dots) with 10-minute mean (thick

solid lines). In this figure, periods of missing data correspond to times

when hydrographic observations were conducted.

Figure 6: Maps of ice thickness averaged for 10 minutes with average ice edges

(broken lines) for (a) 1997 and (b) 1998.

(a) is a case in which ice thickness distribution is different between the

western and eastern regions, while **(b)** is the case in which the difference is small.

Figure 7: Ice thickness distribution each year with the bin width of 10 cm.

(a) 1991 (b) 1992 (c) 1993 (d) 1994 (e) 1996 (f) 1997 (g) 1998

(h) 1999 (i) 2000.

In 1996, the data collected by ILTS and NMRI were integrated because the cruise

tracks were much different and the number of ILTS data were limited to only 153

(see Table 2). In 1999, the broken line shows the ice thickness probability

obtained from the sonar data off Yubetsu. In 2000, the solid and the broken lines

denote the data measured by ILTS and NMRI, respectively, during the same

cruise.

Figure 8: Vertical structure diagrams of first-year ice sampled during 1996 to 2000.

Solid horizontal lines denote the layer boundaries. Broken lines denote

the boundaries where the crystal arrangement is changed due to the growth

process. The values in parentheses are ice thickness (cm). The slanted layers

denote snow ice and excluded from the calculation of H_L in Table 3.

See Figure 3 for the locations of samples.

Figure 9: Frequency distribution of ^{18}O for (a) Columnar ice and (b) Granular ice

with the bin width of 0.1‰

Figure 10: A photograph of typical sea ice area in the southern Sea of Okhotsk,

taken from the helicopter at 10:40 on February 8, 1998. The location is $45^o03.5'N$

$142^o56.2'E$. The side length of the photo corresponds to about 1km.

Figure 11: A schematic illustration to explain the process of our ice model.

Shaded areas are newly rafted ice.   H is the thickness of the unit ice floe.

See text for details.

Figure 12: Comparison of the observed ice thickness distribution

with the Poisson Distributions for   H = 5, 10, and 15 cm as used in equation (3).

(a)1991 (b)1992 (c)1993 (d)1994 (e)1996 (f)1997 (g)1998 (h)1999 (i)2000

Figure 13: Ice thickness distributions in 1999 with the Poisson Distributions

for   H =5, 10, and 15 cm. (a) West of 144.5^{o}E (mean 19.7cm, N=896)

(b) East of 144.5^{o}E (mean 40.0cm, N=762)

Figure 14:

(a) The thickness distribution calculated in our rafting cycle model (a thick solid line).

p and *n* are assumed to be 0.2 and 24 as used in eq. (2), respectively.

The thin line denote the Poisson Distribution for μ =4.8 (0.2× 24) in eq.(3).

Two broken lines denote the calculated thickness distributions when *p* varies at

rafting events with keeping the average being 0.2. Notice that they are nearly the

same as the thick solid line (for constant *p*). See the text for details.

(b) The distribution of components in redistribution functions.

-a(h) and n(h) (both broken lines) are the fractions of the ice

participating in rafting and the newly rafted ice, respectively.

The sum of -a(h) and n(h) (solid line) represents the total change of fraction of

thickness *h*.

Figure 15: Time series of ECMWF wind speed data from December 1 1995

to March 31 1996 at the grid point 47.5^{o}N 145.0^{o}E.

Arrows represent the local maxima in January and February.

Figure 16: The distribution of

(a) the growth rate (cm/day) of congelation ice averaged during three days

(b) the ice production rate (cm/day) over open water.

Both are estimated from heat budget calculation using the meteorological data averaged during late January of 1996 ice growth season. The contour interval is 1 cm/day. See text for details.

Table 1. Daily mean meteorological conditions.

Period (Date in February)	1996 3-5	1997 2-9	1998 4-11	1999 3-10	2000 13-17
Air temp. (^{o}C)	-5.0	-5.4	-8.1	-5.0	-6.6
Relative humidity (%)	74.8	74.9	68.8	80.0	86.5
Solar radiation (W m^{-2})	104.5	108.4	116.6	87.0	86.5
Wind speed (m s^{-1})	6.6	4.3	7.0	6.8	6.7
Cloud amount (tenth)	7.0	6.6	7.5	7.9	8.4

Table 2. Statistics of Ice Thickness.

Year	Period	N	H_{im}(cm)	*s.d.*(cm)	Conducted by
1991	13-14 Feb.	663	29.5	18.1	NMRI
1992	6-7 Feb.	657	25.4	11.5	NMRI
1993	4-8 Feb.	930	44.2	17.7	NMRI
1994	26Jan.-2Feb.	3460	38.8	12.3	NMRI
1996	3-5 Feb.	153	18.5	6.5	ILTS
	23-28 Feb.	8936	29.9	9.8	NMRI
1997	2-9 Feb.	4119	54.9	22.9	ILTS
1998	4-11 Feb.	2910	30.1	12.9	ILTS
1999	3-10 Feb.	1658	29.0	20.4	ILTS
2000	13-17 Feb.	4694	26.9	12.7	ILTS
		2286	28.5	12.3	NMRI
Total			32.7	9.9	

N: Number of samples   Him: Mean ice thickness

s.d.: Standard deviation   NMRI: National Maritime Research Institute

ILTS: Institute of Low Temperature Science

The measurement methods are the same between the two institutes.

The two sets of data in 2000 were obtained during the same cruise.

The total mean ice thickness and s.d. are calculated using the yearly

averaged data. For 1996, both two data sets are included because

their observation areas were different.

Table 3. Statistics of Ice Structure.

year	type	N	c	g	c/g	etc	H_L
1996	first-year ice	1	0	100	0	0	
	young ice	6	0	100	0	0	
	Total	7	0	100	0	0	5.7 cm
1997	first-year ice	4	33	61	4	1	
	young ice	9	52	36	8	4	
	Total	13	42	50	6	3	10.1 cm
1998	first-year ice	3	0	100	0	0	
	young ice	6	18	78	2	2	
	Total	9	10	87	1	1	9.1 cm
1999	first-year ice	4	28	71	0	2	
	young ice	9	14	82	0	4	
	Total	13	21	76	0	3	7.4 cm
2000	first-year ice	2	14	84	2	0	
	young ice	3	31	46	0	23	
	Total	5	21	68	1	10	8.9 cm
Total	first-year ice	14	21	76	2	1	
	young ice	33	24	68	2	5	
	Total	**47**	**22**	**74**	**2**	**3**	**8.2 cm**

(unit: %)

In the table, c,g,c/g, and etc denote columnar ice, granular ice,

mixture of c and g, and other structure, respectively.

N and H_L means the number of samples and the average one layer thickness.

Snow ice layer was excluded from the calculation of H_L.

Table 4. Evolution of ice thickness distribution

Time Step (n)	Ice Thickness (m× H)				
	1	**2**	**3**	**4**	**5**
0	1	0	0	0	0
1	$1-p$	p	0	0	0
2	$(1-p)^2$	$2p(1-p)$	p^2	0	0
3	$(1-p)^3$	$3p(1-p)^2$	$3p^2(1-p)$	p^3	0
4	$(1-p)^4$	$4p(1-p)^3$	$6p^2(1-p)^2$	$4p^3(1-p)$	p^4

Figure 1: Map of the southern Okhotsk Sea with the ship tracks for 1996-2000 with

the mean ice edges on February 10 for 1971 to 2000 (thick broken line).

The mean ice edges are adopted from the *Japan Meteorological Agency* [2001].

The triangle marks the location of ice thickness monitoring by upward-looking

sonar in 1999 winter. The water depth there is 58 m.

Figure 2: Ice thickness measurement by video monitoring.

 Schematic diagram of observation technique (after *Shimoda et al.*, 1997).

Figure 3: Locations of young and first-year ice samples which were collected

from 1996 to 2000. The broken lines denote the mean ice edges on February 10

for 1971 to 2000. The numbers in bold correspond to the first-year ice samples

illustrated in Figure 8.

1: 96A, 2: 97A, 3: 97B, 4: 97C, 5: 97D, 6: 98A, 7: 98B, 8: 98C, 9: 99A

10: 99B, 99D 11: 99C, 12: 2000A, 13: 2000B.

Figure 4: Samples of thick (a) and thin (b) sections.

This is a sample of 40 cm thick ice taken in 1997, corresponding to 97A in Figure 8.

Note that columnar ice is sandwiched between granular ice at three locations,

suggesting the importance of a dynamic accumulation process. The arrows show

the boundaries of layers used for the calculation of H_L in Table 3.

The thick ice (5mm) structure revealed by the scattered light.

The thin section (< 1mm) illuminated between crossed polarizers.

Figure 5: Ice thickness data.

An example of time series of ice thickness data (dots) with 10-minute mean (thick

solid lines). In this figure, periods of missing data correspond to times

when hydrographic observations were conducted.

Figure 6: Maps of ice thickness averaged for 10 minutes with average ice edges

(broken lines) for (a) 1997 and (b) 1998.

(a) is a case in which ice thickness distribution is different between the

western and eastern regions, while **(b)** is the case in which the difference is small.

Figure 7: Ice thickness distribution each year with the bin width of 10 cm.

(a) 1991 (b) 1992 (c) 1993 (d) 1994 (e) 1996 (f) 1997 (g) 1998

(h) 1999 (i) 2000.

In 1996, the data collected by ILTS and NMRI were integrated because the cruise

tracks were much different and the number of ILTS data were limited to only 153

(see Table 2). In 1999, the broken line shows the ice thickness probability

obtained from the sonar data off Yubetsu. In 2000, the solid and the broken lines

denote the data measured by ILTS and NMRI, respectively, during the same cruise.

Figure 8: Vertical structure diagrams of first-year ice sampled during 1996 to 2000.

Solid horizontal lines denote the layer boundaries. Broken lines denote the boundaries

where the crystal arrangement is changed due to the growth process. The values in

parentheses are ice thickness (cm). The slanted layers denote snow ice and excluded

from the calculation of H_L in Table 3. See Figure 3 for the locations of samples.

Figure 9: Frequency distribution of ^{18}O for (a) Columnar ice and (b) Granular ice

with the bin width of 0.1‰

Figure 10: A photograph of typical sea ice area in the southern Sea of Okhotsk,

taken from the helicopter at 10:40 on February 8, 1998. The location is $45^o03.5'N$

$142^o56.2'E$.   The side length of the photo corresponds to about 1km.

Figure 11: A schematic illustration to explain the process of our ice model.

Shaded areas are newly rafted ice. H_B is the thickness of the unit ice floe.
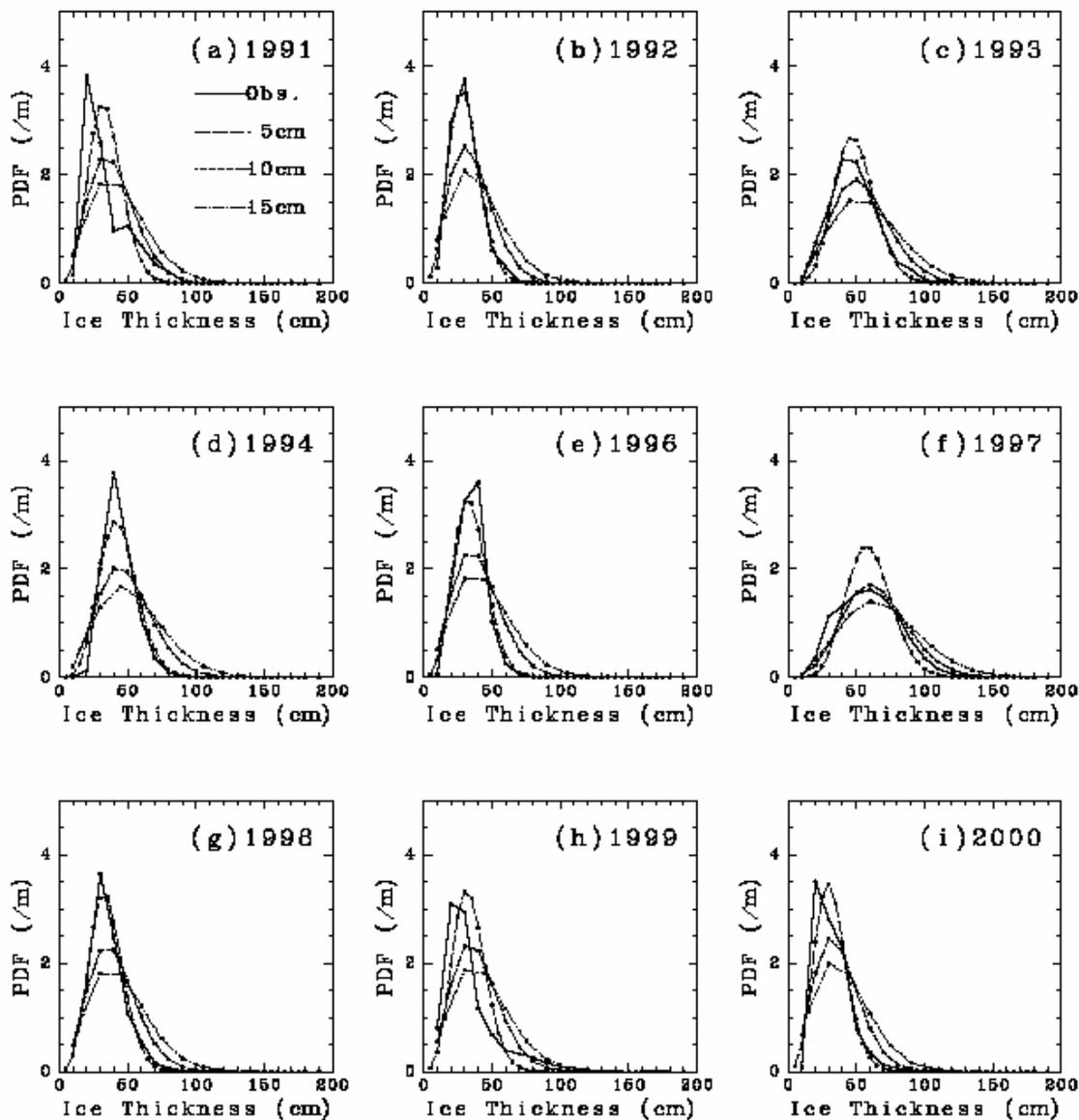
See text for details.

Figure 12: Comparison of the observed ice thickness distribution

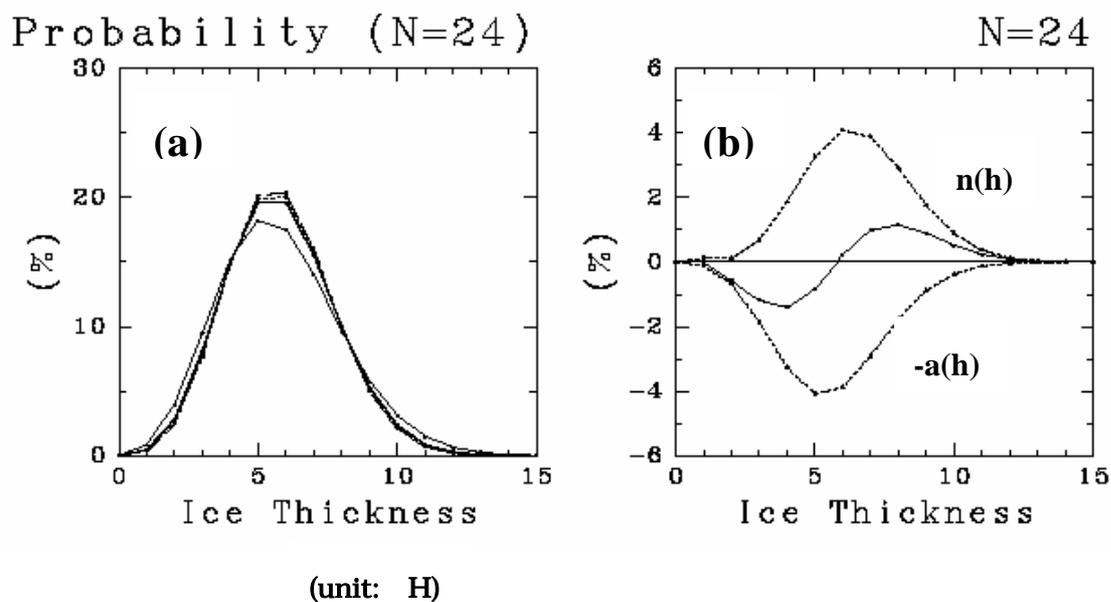with the Poisson Distributions for H_B = 5, 10, and 15 cm as used in equation (3).
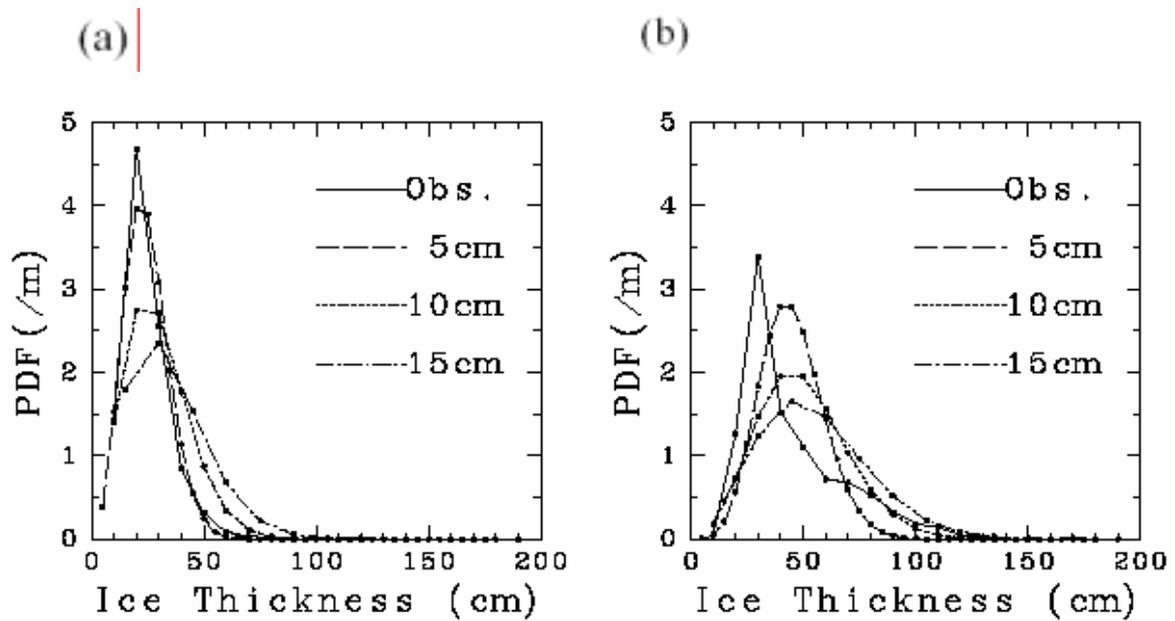
(a)1991 (b)1992 (c)1993 (d)1994 (e)1996 (f)1997 (g)1998 (h)1999 (i)2000

Figure 13: Ice thickness distributions in 1999 with the Poisson Distributions

for H =5, 10, and 15 cm. (a) West of 144.5°E (mean 19.7cm, N=896)

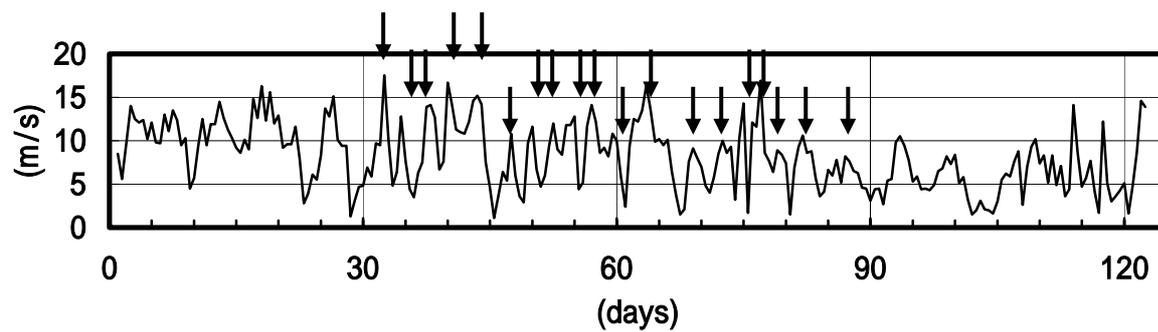(b) East of 144.5°E (mean 40.0cm, N=762)

Figure 14:

(a) The thickness distribution calculated in our rafting model (a thick solid line).

p and *n* are assumed to be 0.2 and 24 as used in eq. (2), respectively. The thin line denote

the Poisson Distribution for μ =4.8 (0.2x24) in eq.(3). Two broken lines denote the

calculated thickness distributions when *p* varies at rafting events with keeping the

average being 0.2. Notice that they are nearly the same as the thick solid line

(for constant *p*). See the text for details.

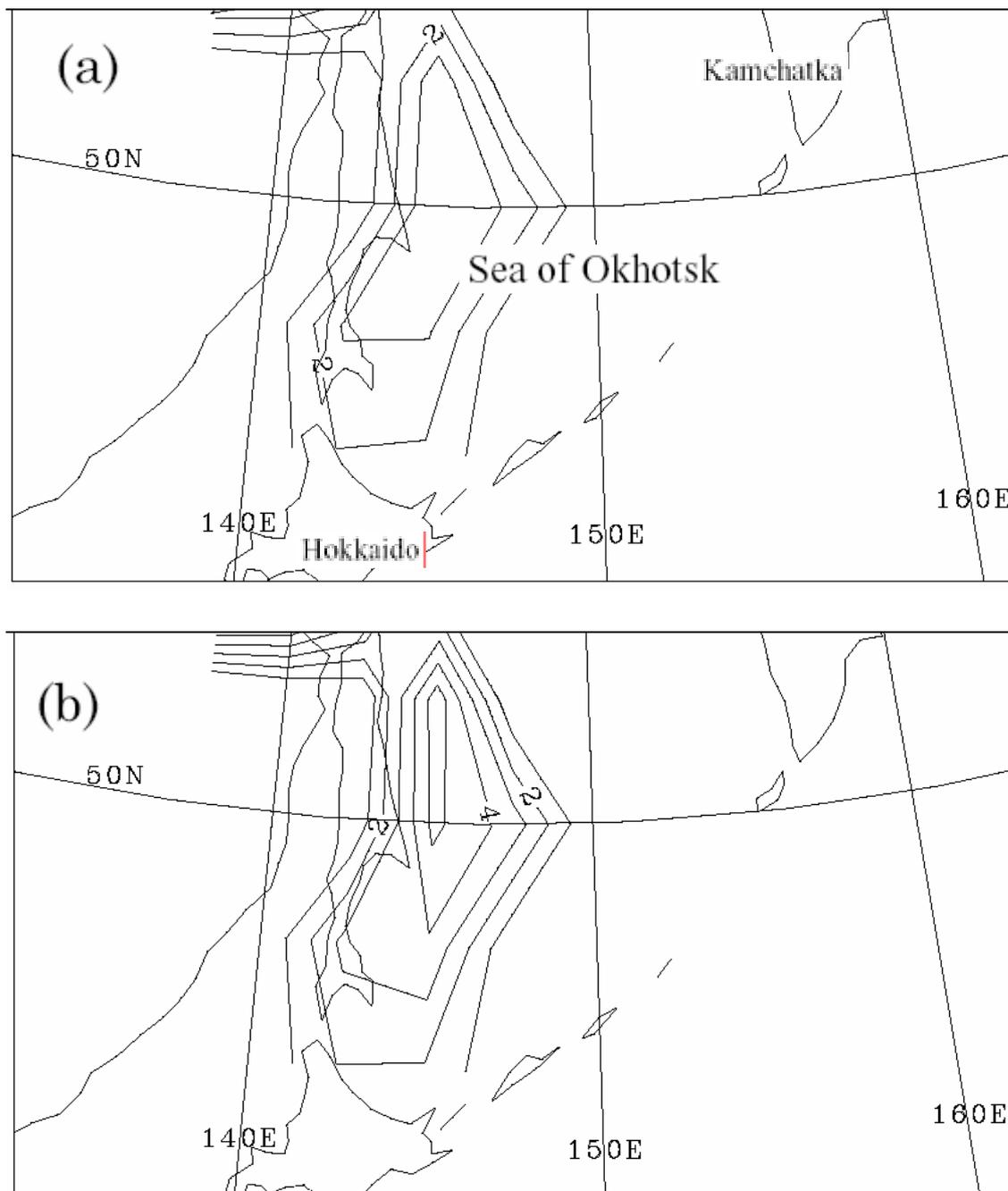(b) The distribution of components in redistribution functions.

-a(h) and n(h) (both broken lines) are the fractions of the ice participating in rafting and

the newly rafted ice, respectively. The sum of -a(h) and n(h) (solid line) represents the

total change of fraction of thickness *h*.

Figure 15: Time series of ECMWF wind speed data from December 1 1995

to March 31 1996 at the grid point 47.5^{o}N 145.0^{o}E.

Arrows represent the local maxima in January and February.

Figure 16: The distribution of (a) the growth rate (cm/day) of congelation ice averaged during

three days and (b)the ice production rate (cm/day) over open water.

Both are estimated from heat budget calculation using the meteorological data averaged

during late January of 1996 ice growth season. The contour interval is

1 cm/day. See text for details.